Magnetism in bcc and fcc Fe with carbon and manganese

2010 J. Phys.: Condens. Matter 22 316002

(http://iopscience.iop.org/0953-8984/22/31/316002)

J. Phys.: Condens. Matter **22** (2010) 316002 (7pp) doi:10.1088/0953-8984/22/31/316002

Magnetism in bcc and fcc Fe with carbon and manganese

N I Medvedeva[1,2], D Van Aken[2] and J E Medvedeva[3]

[1] Institute of Solid State Chemistry, Yekaterinburg 620990, Russia
[2] Department of Materials Science and Engineering, Missouri University of Science and Technology, Rolla, MO 65409, USA
[3] Department of Physics, Missouri University of Science and Technology, Rolla, MO 65409, USA

Received 16 March 2010, in final form 17 June 2010
Published 8 July 2010
Online at stacks.iop.org/JPhysCM/22/316002

Abstract
Density functional theory calculations were performed to study the structure and magnetic properties of bcc (α) and fcc (γ) Fe with 3 at.% carbon and manganese impurities. We find that all bcc-based Fe, Fe–C and Fe–Mn–C phases exhibit a ferromagnetic (FM) ground state, while the antiferromagnetic double-layer (AFMD) state is lowest in energy within the collinear spin approach in fcc Fe, Fe–C and Fe–Mn–C phases. However, the carbon and manganese impurities affect the local magnetic interactions significantly. The states with opposite manganese magnetic moments are quasi-degenerate in bcc Fe–Mn alloy, whereas octa-site carbon stabilizes ferromagnetic coupling of the nearest manganese atom with the Fe host. We demonstrate that the antiferromagnetic (AFM) fcc Fe–C and Fe–Mn–C alloys are intrinsically inhomogeneous magnetic systems. Carbon frustrates the local magnetic order by reorientation of magnetic moments of the nearest Mn and Fe atoms, and favors their ferromagnetic coupling. The competition between ferromagnetic and antiferromagnetic Fe–Fe and Fe–Mn interactions and the local magnetovolume instability near carbon may give rise to the spin-glass-like regions observed in austenitic Fe–Mn–C alloys.

(Some figures in this article are in colour only in the electronic version)

1. Introduction

Carbon and manganese are the two most important additions in iron alloys, which determine the main properties of steels and cast irons. Carbon is responsible for hardness and tensile strength, while manganese acts as a carbide stabilizer and also eliminates harmful oxide and sulfurous compounds of iron. Both impurities affect the mechanics and kinetics of the α–γ phase transformation. They sharply lower the temperature of this transition and act as austenite stabilizers. Advanced austenitic Fe–Mn–C steels have exceptional formability and high strength and are of growing importance in making lightweight automobiles [1]. Furthermore, interest in the Fe–Mn–C alloys is also due to the development of the hard bainitic steels where the high hardness and strength result from a nanoscale duplex ferrite–austenite structure of carbide-free bainite [2, 3].

The complex structural and magnetic phase diagram of iron makes it challenging to determine the effect of impurities on the microstructure of alloys as well as its electronic structure, which is critical for the fundamental understanding of the observed macroscopic properties. It is known that the ground state of bcc Fe is ferromagnetic (FM) and fcc Fe is paramagnetic within the temperatures of thermodynamic stability (1184–1665 K), while the spin-spiral antiferromagnetic structure was found for the Fe precipitates stabilized in a Cu matrix [4]. The electronic structure of bcc and fcc Fe has been intensively investigated in many theoretical studies [6–19], and various magnetic states in fcc Fe were found to have slightly different volumes and comparable total energies that lead to their competition.

Both the phase stability and magnetism in the Fe-based alloys are sensitive to alloying elements and their concentrations. Depending on the manganese content, the Fe–Mn alloys exhibit γ–α (fcc–bcc) or γ–ϵ (fcc–hcp) martensitic transformations, which are closely related to the magnetic properties [20]. At a small content, manganese in bcc Fe alloys was experimentally shown to have either ferromagnetic [21, 22] or antiferromagnetic coupling with iron [23], and the fluctuations between these

Table 1. Optimized lattice parameters (a and c/a), total energy difference between NM and FM states (ΔE) and local magnetic moments (m) for bcc Fe, bct Fe–C and Fe–Mn–C phases. For comparison, previous theoretical data: for NM and FM bcc Fe, the lattice parameters a are 2.77 and 2.84 Å [17], 2.76 and 2.83 Å [39]; the magnetic moment is 2.17 μ_B [17] or 2.20 μ_B [39], respectively.

	Fe		Fe32C		Fe31MnC	
	NM	FM	NM	FM	NM	FM
a (Å)	2.76	2.84	2.47	2.82	2.47	2.82
c/a	1.00	1.00	1.39	1.04	1.39	1.04
ΔE (meV/atom)	451	0	158	0	112	0
m (Mn) (μ_B)	—	—	—	—	—	1.0
m (FeI) (μ_B)	—	2.2	—	1.7	—	1.6
m (FeII) (μ_B)	—	2.2	—	2.2	—	2.2

degenerate states were thought to explain the contradictory observations [24, 25]. *Ab initio* calculations demonstrated that the Mn–Fe coupling in bcc $Fe_{1-x}Mn_x$ alloys is antiferromagnetic in the dilute limit [26] and the reorientation of manganese magnetic moment was predicted to occur for $x > 3$ at.% in ordered [27] and for $x > 10$ at.% in disordered alloys [26]. In fcc Fe–Mn alloys, the experimental finding [28] of AFM order was confirmed theoretically [26, 29–32], and different magnetic states (helical, non-collinear and single-layer AFM states) were found to exhibit strong volume and concentration dependences [32].

The Fe–C phase diagram is complex and depends strongly on the carbon content and heat treatment. The carbon solubility in the interstitial fcc Fe–C alloy (austenite) reaches up to 10 at.%, while in bcc Fe–C (ferrite) it is less than 0.1 at.% and higher carbon content is observed in body-centered tetragonal (bct) Fe–C alloy (martensite) instead of the cubic one [33]. As distinct from the Fe and Fe–Mn phases, few theoretical studies are available for the Fe–C and Fe–Mn–C alloys [34–40], and their phase stability and magnetism are not well established. The observed anomalies in magnetic susceptibility indicate the occurrence of inhomogeneous ferromagnetic and spin-glass-like regions in fcc Fe–Mn–C alloys [41]. Recent *ab initio* calculations [40] reveal a ferromagnetic local ordering near carbon in fcc Fe–C and predict the change in crystal structure and ground magnetic state from tetragonal double-layer antiferromagnetic (AFMD) to cubic ferromagnetic with the addition of 3 at.% carbon. However, this result contradicts the widely accepted belief that the transition to the ferromagnetic state occurs only at 10 at.% [33] and further *ab initio* investigations are required for the Fe–C and Fe–Mn–C alloys.

In this work we perform comparative investigations of the electronic structure and magnetic properties of bcc and fcc Fe, and their solid solutions with interstitial carbon and substitutional manganese. The main goal is to determine the ground states of the Fe–C and Fe–Mn–C phases with low manganese and carbon concentrations and to understand how these impurities affect the lattice parameters, local crystal structure and magnetic interactions. The magnetic order and ground state of the Fe-based alloys are known to be sensitive to the choice of theoretical approach and the exchange–correlation potential [19, 25, 42]. Hence, it is important

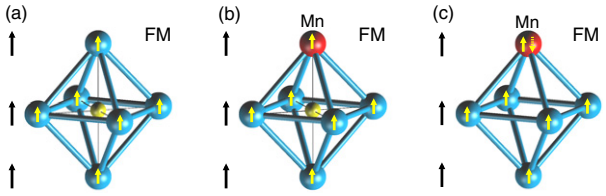

Figure 1. Local magnetic coupling of the Fe (blue) and Mn (red) atoms which are nearest to the interstitial carbon (yellow) in (a) CFe6 octahedron in bct Fe–C alloy, (b) CFe5Mn octahedron in bct Fe–Mn–C alloy and (c) Fe5Mn octahedron in bcc Fe–Mn alloy. Black arrows at the left show layer magnetic ordering in bulk.

to study both phases within one *ab initio* scheme. For this, we used the projector augmented waves (PAW) method as implemented in the Vienna *ab initio* simulation package (VASP) [43, 44] and the PBE functional [45] for the exchange and correlation energy. The calculations were performed with a $16\times16\times16$ k-point mesh for bcc and fcc Fe, and a $6\times6\times6$ k-point mesh for Fe–C and Fe–Mn–C. Note that, in order to compare results with the same impurity concentration, we used the 32-atom supercells FeXMnYCZ (X, Y and Z denote the number of corresponding atoms in the supercell) for both bct and fcc phases. We considered the ordered configuration with the octahedral interstitial sites for carbon, which are the most preferable in both Fe phases [33, 39], and the nearest substitutional positions of manganese. The lattice parameters and the internal positions of all atoms in supercells were optimized by the atomic forces and total energy minimization.

2. Carbon and manganese in bcc Fe

For pure bcc Fe we obtained a ferromagnetic ground state with the lattice parameter and the local magnetic moment being in good agreement with experimental [5, 33] and previous theoretical results, table 1. Interstitial octa-site carbon in bcc Fe induces a tetragonal distortion, which depends strongly on the carbon concentration and decreases from 1.076 for Fe16C to 1.019 for Fe54C [39]. For FM Fe–3 at.% C (Fe32C), we obtained c/a of 1.037 (table 1), which agrees with the observed variation of lattice parameter with carbon content x in martensite, namely $a = a_\alpha - 0.003x$ and $c/a = 1 + 0.0099x$, where x is in at.% [33]. Octa-site carbon has two apical FeI and four planar FeII atoms in the CFe6 octahedron (figure 1). The FeI–C distances increase upon relaxation to 1.79 Å, while the FeII–C distances, 1.98 Å, remain nearly the same—as compared to the unrelaxed values of 1.42 and 2.00 Å in bcc structure, respectively. Magnetic moments of the nearest FeI atoms decrease (table 1), whereas the total magnetization increases up to 2.4 μ_B due to the increased number of valence electrons and a larger volume of the Fe–C phase [33, 46].

Manganese in the tetragonally distorted CFe6 octahedron prefers to substitute the apical FeI atom, while the replacement of FeII is higher in energy by 26 meV. No evident changes in the lattice parameters and local distortions were found for 3 at.% of manganese, and both Mn and FeI atoms are located at the same distance of 1.79 Å from the carbon. Significantly, we obtained one stable magnetic state with

Table 2. Optimized lattice parameters (a and c/a), total energy difference between phases (ΔE) and local magnetic moments (m) for cubic (c) and tetragonal (t) fcc Fe. For comparison, previous theoretical data: for cubic FM/LS, FM/HS, AFM1 and AFMD, the lattice parameters a are 3.49, 3.64, 3.50 and 3.53 Å [17], and 3.47, 3.64, 3.48 and 3.52 Å [39]; the magnetic moments are 1.02, 2.57, 1.30 and 1.80 μ_B [17], and 0.94. 2.62, 1.23 and 1.79 μ_B [39], respectively. For tetragonal FM/HS, AFM1 and AFMD the lattice parameters a are 3.35, 3.47 and 3.49 Å [6], and 3.58, 3.44 and 3.57 Å [40]; c/a are 1.20, 1.08 and 1.08 Å [6], and 1.08, 1.09 and 1.05 [40]; magnetic moments are 2.5, 1.8 and 2.3 μ_B [40]; ΔE are 33, 45 and 0 meV/atom [40], respectively.

	NM	FM/LS-c	FM/HS-c	FM/HS-t	AFM1-c	AFM1-t	AFMD-c	AFMD-t
a (Å)	3.45	3.47	3.64	3.43	3.48	3.42	3.53	3.46
c/a	1.00	1.00	1.00	1.17	1.00	1.07	1.00	1.08
ΔE, (meV/atom)	76	69	72	19	37	17	27	0
m (Fe) (μ_B)	—	1.0	2.5	2.4	1.2	1.6	1.8	2.0

ferromagnetically coupled manganese in Fe5MnC octahedron (table 1 and figure 1), which is in contrast to bcc Fe31Mn, where there are two stable states with the opposite manganese magnetic moments of -1.9 and 1.0 μ_B, which differ in energy only by 3 meV/atom. A small energy difference between the ferromagnetic and antiferromagnetic states of Mn in bcc Fe has been obtained in previous single-impurity calculations [24, 25], and fluctuations between these two states were suggested. The equal number of Mn atoms with the opposite spin orientation was also predicted for Mn content of 2 at.% [27]. Thus, the competition between the FM and AFM Mn–Fe coupling occurs in the Fe–Mn alloys for an Mn concentration of about 2–3 at.%, while carbon stabilizes the ferromagnetic interaction between the nearest Mn and Fe atoms.

3. Carbon and manganese in fcc Fe

For fcc Fe we performed calculations for nonmagnetic (NM), ferromagnetic, single-layer antiferromagnetic (AFM1) and double-layer antiferromagnetic (AFMD) states. It should be noted that the AFMD state with extra intralayer ferromagnetic coupling is a good collinear approximation for spiral magnetism and describes the properties of fcc Fe better than the AFM1 structure [9, 17]. The cubic symmetry and collinear magnetism are incompatible [33] and to elucidate the effect of tetragonality, which was suggested to be important in fcc Fe [6, 40], we studied both cubic and tetragonal structures with the fixed lattice symmetry. For every magnetic state, we obtained the tetragonal equilibrium structure to be lower in energy than the corresponding cubic phase by 27–45 meV/atom (table 2). This finding is in agreement with the $c/a > 1$ tetragonality of all magnetic fcc Fe phases [6, 40].

We obtained that the AFMD state is the most stable collinear state in fcc Fe, in accord with previous studies [17, 19, 39, 40]. The considered magnetic states have comparable equilibrium volumes and total energies that may result in their competition, as was established in numerous theoretical studies. The magnetovolume instability in fcc Fe, which involves the low-spin (LS) and higher-energy high-spin (HS) FM states, was traditionally considered as a mechanism of the anti-Invar effect [47]. Indeed, for cubic structures we found that the FM/HS state is higher in energy than the FM/LS state, as well as obtained in previous calculations [17, 39, 47]. However, we found that the tetragonal HS state (note that we did not obtain any stable tetragonal FM/LS state) is much lower than the cubic LS state at the equilibrium volumes differing by 13% (table 2). This volume difference significantly overestimates the observed volume expansion of 7% [5], while the transformation from AFMD to FM/HS is energetically more favorable and corresponds to a much better agreement with volume expansion. Transformation between AFM and FM/HS has been suggested [17] for interpretation of the anti-Invar effect and recent *ab initio* calculations demonstrate that a non-collinear state may be involved as well [9, 48].

Following [17], we related the energy difference between the ground states of bcc and fcc Fe with the α–γ transition temperature and obtained 1006 K, which is close to the experimental value of 1183 K. Such an estimation does not include the entropy contributions but, nonetheless, it gives a reasonable transition temperature (see also [17]) since the energy difference is examined between magnetic phases at zero pressure [50]. We note that the energy difference between the nonmagnetic α-Fe and γ-Fe phases is more than three times larger (3447 K) and has opposite sign, which points to the crucial role of magnetic interaction in this transition.

We obtained that interstitial octa-site carbon lowers the total energy difference between bcc and fcc Fe phases and the α–γ transformation temperature reduces to 951 K. This correlates with the trend in the equilibrium phase diagram of Fe–C [46], where a temperature of about 970 K was observed for a carbon concentration of 3 at.%. Similar to fcc Fe, the interstitial fcc Fe–C alloy also demonstrates an anti-Invar behavior at a low carbon concentration [5]. The transition from AFMD to FM/HS in fcc Fe–3 at.% C corresponds to smaller energy and volume expansion (5%) as compared to fcc Fe. Further increase in carbon concentration up to its solubility limit of 10%, where the ground state is ferromagnetic, results in the disappearance of the anti-Invar effect [33].

Carbon in fcc Fe reduces the difference between the total energies of cubic and tetragonal structures (cf tables 2 and 3) and the ground cubic AFMD state is almost degenerate with the tetragonal FM and AFM1 as well as with cubic AFM1 states. The largest energy difference between the tetragonal and cubic phases was obtained for the FM state, while these phases in the AFM state have similar equilibrium volumes and total energies. In agreement with [39], we did not obtain any stable FM/LS state in fcc Fe–C, and a possible reason for this is the volume expansion caused by the presence of octa-site carbon.

Interstitial carbon at 3 at.% concentration reduces the energy difference between the AFMD and other magnetic states (tables 2 and 3) but does not change the ground state of fcc Fe, which remains AFMD according to our collinear

Table 3. Optimized lattice parameters (a and c/a), total energy difference between phases (ΔE) and local magnetic moments (m) for cubic (c) and tetragonal (t) fcc Fe–C phases. For comparison, previous theoretical data: for tetragonal FM, AFM1, AFMD states, the lattice parameters a are 3.73, 3.56 and 3.61 Å, and c/a are 0.97, 1.04 and 1.00; the magnetic moments are 2.7, 1.9 and 2.1 μ_B, ΔE are 0, 47 and 16 meV/atom [40], respectively.

	NM	FM/HS-c	FM/HS-t	AFM1-c	AFM1-t	AFMD-c	AFMD-t
a (Å)	3.47	3.65	3.46	3.51	3.47	3.55	3.48
c/a	1.00	1.00	1.15	1.00	1.05	1.00	1.08
ΔE (meV/atom)	65	52	17	15	12	16	0
m (FeI) (μ_B)	—	2.1	2.2	$1.1^{\uparrow}$	$1.5^{\uparrow}$	$0.3^{\uparrow}$, $-2.0^{\downarrow}$	$1.3^{\uparrow}$, $-2.0^{\downarrow}$
m (FeII) (μ_B)	—	2.1	2.0	$1.1^{\downarrow}$	$1.1^{\downarrow}$	$1.3^{\uparrow}$	$1.5^{\uparrow}$

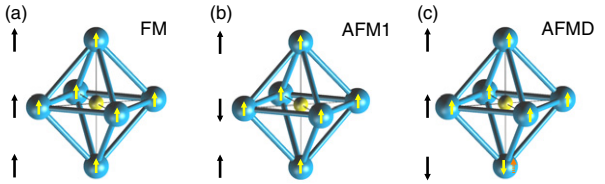

Figure 2. Local magnetic coupling of the Fe (blue) atoms which are nearest to interstitial carbon (yellow) in fcc Fe–C alloy for (a) FM, (b) AFM1 and (c) AFMD states. Black arrows at the left show the layer magnetic ordering in bulk.

calculations (table 3). Indeed, the ground FM state is expected only above the solubility limit of carbon (10 at.%) [33, 46]. This differs from the calculations [40], where the high-spin FM state was found to be lower than the AFM1 and AFMD states in Fe–3 at.% C. The disagreement between our results and those from [40] is likely to appear from the different lattice parameters obtained for the Fe32C supercell. According to our calculations, carbon only slightly affects c/a for all magnetic states, whereas a very strong decrease in c/a from 1.08, 1.09 and 1.05, to 0.97, 1.04 and 1.00 for the FM, AFM1 and AFMD states, respectively, was predicted in [40], where structural optimization was performed within SIESTA and LMTO-ASA methods.

For the AFMD state, we found that all Fe atoms have FM coupling with other atoms in the layers they belong to. As a result, five iron atoms in the CFe6 octahedron are ferromagnetically coupled with each other and one FeI atom has an opposite spin (it belongs to a layer of different spin alignment, table 3 and figure 2). The magnetic moments of the two FeI atoms are different and the largest moment of -2.0 μ_B corresponds to FeI most remote from carbon. In addition, we obtained another stable AFMD configuration in which all six Fe atoms in the octahedron are FM-coupled and which is higher in energy by 6 meV/atom. In this state, both FeI atoms are at the same distances from carbon and have almost equal magnetic moments of 1.7 and 1.9 μ_B. Notice that the magnitude of the reoriented FeI moment remains the same (-2.0 μ_B versus 1.9 μ_B). Similar results were obtained for the cubic AFMD phase, where there are two stable states with five and six FM-coupled Fe atoms in the CFe6 octahedron. In this case, the energy for spin reorientation—i.e. the energy difference between the two magnetic states—is less than 1 meV/atom.

In the AFM1 state, the FeI and FeII atoms belong to the layers with opposite spin directions, figure 2. We find that two FeI atoms have similar magnetic moments as in AFM1 fcc Fe, whereas the moments of four FeII atoms have opposite directions with respect to the other Fe atoms in the layer (figure 2). Therefore, carbon frustrates the ideal magnetic order of the AFM1 state by spin reorientation of the nearest iron atoms to make them ferromagnetically coupled in the CFe6 octahedron. Here we stress that in the AFM1 state all six Fe atoms near carbon have the same spin directions, whereas only five are FM-coupled in the lowest-energy AFMD state where additional intralayer ferromagnetic interactions are already present in the double-layer antiferromagnetic structure [17].

The carbon-induced tendency to form local ferromagnetic Fe clusters can be demonstrated by calculating the exchange interaction parameters which describe character (i.e. ferromagnetic vs antiferromagnetic) and the strength of the exchange coupling. Previously, the exchange interaction parameters were calculated for FM Fe–3 at.% C with tetragonality of $c/a = 0.97$ [40]. For the optimized AFM1 structure, which we find to be lower in energy, table 3, we obtain[4] that all iron atoms in the octahedron are ferromagnetically coupled with the exchange parameters $J_{\mathrm{FeI-FeII}} = 21$ K, $J_{\mathrm{FeI-FeI}} = 38$ K and $J_{\mathrm{FeII-FeII}} = 19$ K. These parameters have the same sign, but are smaller than those calculated in [40], namely 80–130 K. The coupling between the FeII atoms and their nearest iron atoms in the layer (i.e. next-nearest Fe neighbors of carbon) is AFM with the calculated exchange parameter of 80 K which is close to 83 K for the nearest Fe atoms in fcc Fe [40]. Thus, our calculated exchange interaction parameters confirm that the presence of carbon favors the local ferromagnetic coupling of its neighboring Fe atoms in fcc Fe.

To understand the changes in electronic properties associated with the carbon-induced reorientation of Fe magnetic moments, we analyzed the density of states for AFM1 Fe32C. Our calculations reveal a substantial redistribution of the spin-resolved density of states for FeII atoms (figure 3). An important feature in the FeII(3d) DOS is the enhancement of the spin-up states from -0.5 eV up to the Fermi level, E_F, and the narrowing of the spin-down peak above E_F associated with antibonding FeII(3d) states. As a result, the Fermi level falls at a sharply decreasing slope of the spin-up FeII(3d) DOS. A negative slope near the

[4] The effective exchange interaction parameters were calculated within the TB-LMTO-ASA method [51] as the second derivative of the total energy with respect to the angle of magnetic moment rotation, see [52].

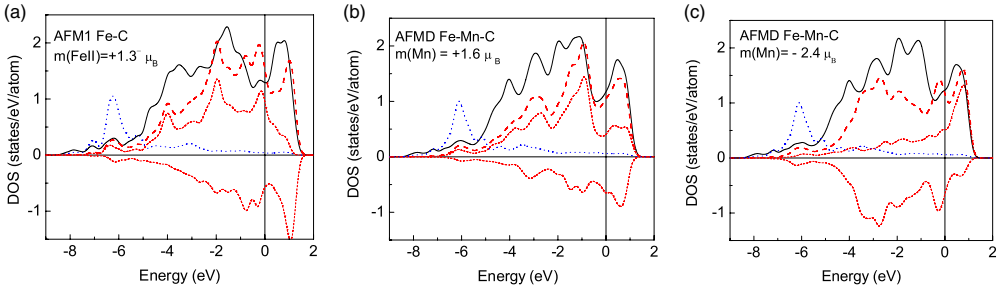

Figure 3. Total density of states (solid black line) and local densities of states for carbon (dotted blue line) for (a) FeII 3d (dashed red line) or for ((b) and (c)) Mn 3d (dashed red line) in AFM1 Fe32C or AFMD Fe31MnC, respectively. The spin-resolved densities of states for FeII and Mn are also shown (dotted red lines). The total energy difference between the positive (b) and negative (c) orientation of manganese spin direction is only 2 meV/atom.

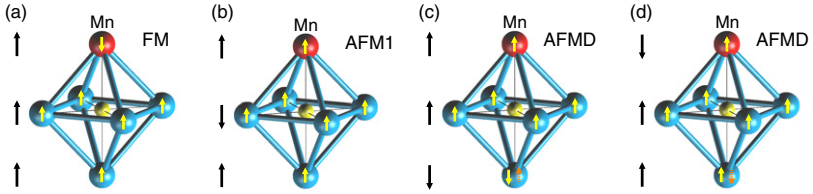

Figure 4. Local magnetic coupling of the Fe (blue) and Mn (red) atoms which are nearest to interstitial carbon (yellow) in fcc Fe–Mn–C alloy for (a) FM, (b) AFM1 and (c) AFMD states with Mn and C being in layers with the same spin direction, (d) AFMD state with Mn and C being in layers with the opposite spin direction. Black arrows at the left show the layer magnetic ordering in bulk.

Table 4. Optimized lattice parameters (a and c/a), total energy difference between phases (ΔE) and local magnetic moments (m) for cubic (c) and tetragonal (t) fcc Fe–Mn–C phases.

	NM	FM/HS-c	FM/HS-t	AFM1-c	AFM1-t	AFMD-c	AFMD-t
a (Å)	3.47	3.65	3.47	3.53	3.47	3.55	3.48
c/a	1.00	1.00	1.15	1.00	1.05	1.00	1.08
ΔE (meV/atom)	63	53	26	14	11	16	0
m (Mn) (μ_B)	—	−2.4	−2.4	$0.1^{\uparrow}$	$1.4^{\uparrow}$	$1.0^{\uparrow}$	$1.6^{\uparrow}$
m (FeI) (μ_B)	—	2.0	2.1	$1.0^{\uparrow}$	$1.4^{\uparrow}$	$-1.9^{\downarrow}$	$-1.9^{\downarrow}$
m (FeII) (μ_B)	—	2.0	2.0	$1.0^{\downarrow}$	$1.0^{\downarrow}$	$1.3^{\uparrow}$	$1.6^{\uparrow}$

Fermi level is believed to drive the system toward magnetic instability. Indeed, the antiferromagnetic state is known to be unstable with respect to the ferromagnetic state under volume expansion associated with a temperature increase or impurity concentration.

Manganese in all tetragonal austenitic phases prefers to substitute for FeI in the distorted octahedron and has antiparallel and parallel direction of magnetic moment relative to the Fe matrix in FM and AFM states, respectively (table 4). We find that manganese increases the energy difference between the AFM and FM states. Previous calculations also gave the positive Mn magnetic moment in AFM Fe–Mn alloy and the manganese-induced suppression of FM order [26]. Similar to fcc Fe and fcc Fe–3 at.% C, the tetragonal AFMD structure is a ground state for fcc Fe with the 3 at.% addition of manganese and carbon. Based on our results, the α–γ transformation temperature decreases to 805 K, which is in accord with the well-known shift of transition to lower temperatures due to manganese addition (manganese is an austenite-stabilizing element). Assuming linear concentration–temperature dependence, we find that about 10 at.% Mn may shift this transition to room temperature, which corresponds well with Hadfield's original work on high manganese steel [49].

The reorientation of iron magnetic moments induced by carbon also persists for austenite with 3 at.% manganese. Similar to AFM1 Fe–C, in AFM1 Fe–Mn–C the nearest FeII atoms have opposite spins with respect to the other Fe atoms in the layer, figure 4(b). Our calculated exchange parameters, $J_{\mathrm{FeI-FeII}} = 7$ K, $J_{\mathrm{FeI-Mn}} = 46$ K and $J_{\mathrm{FeII-FeII}} = 4$ K, prove the FM interactions in the CMnFe5 octahedron, whereas the coupling between the FeII atoms and their nearest iron atoms in the layer (i.e. next-nearest Fe neighbors of carbon) is AFM with an exchange parameter of 46 K. In this case we obtained the reduced exchange parameters for Fe–Fe pairs in comparison with exchange parameters in fcc Fe–C, which demonstrate the suppression of ferromagnetism by manganese.

For the AFMD structure we obtained two quasi-degenerate states with opposite FeI spins, figure 4(c). The FeI spin flip in the AFMD state makes all six atoms ferromagnetically coupled in the octahedron (the magnetic moments of Mn, FeI and FeII atoms are 1.8, 1.9 and 1.6 μ_B, respectively) and requires only 5 meV/atom. We

found another stable AFMD configuration, where the Mn and C atoms belong to layers of the opposite spin alignment and manganese has antiferromagnetic intralayer coupling, figure 4(d). In this AFMD state, which is higher by 2 meV/atom, the Mn, FeI and FeII atoms in the octahedron are ordered ferromagnetically (the magnetic moments are -2.4, -1.6 and -1.6 μ_B, respectively). A comparison of the calculated densities of states for AFMD Fe–Mn–C structures with two orientations of manganese magnetic moment reveals a substantial redistribution in the partial DOS for the Mn atom with antiparallel spin, figure 3. Similar to DOS for the spin-flipped FeII atom in fcc Fe–C, figure 3, the Fermi level falls at the negative slope of the Mn 3d spin-up states in fcc Fe–Mn–C with negative manganese moment (figure 3(c)), whereas the DOS for Mn with positive magnetic moment (figure 3(d)) resembles the DOS of all other Fe atoms.

For cubic AFMD structure, our calculations also gave the additional stable states with the flipped iron and manganese magnetic moments. Furthermore, we obtained the second stable FM state with the manganese moment of 1.9 μ_B, which is higher than the ground FM state (where the Mn moment is -2.4 μ_B) by 5 meV/atom. All six atoms near carbon are ferromagnetically coupled in this quasi-degenerate state.

Thus, in contrast to the fcc Fe–Mn alloy, where magnetic instability exists for the Fe moments but not for the Mn moments [26, 29], in fcc Fe with 3 at.% additions of Mn and C the spin flip is possible in the $(Fe, Mn)_6C$ octahedron for both iron and manganese—i.e. both can have either ferromagnetic or antiferromagnetic coupling with the Fe matrix in the FM and AFMD states. The spin fluctuations may be more pronounced in a non-collinear magnetic state, thus, favoring the appearance of the spin-glass regions where the exchange interactions may have a random sign.

4. Summary

Using an *ab initio* approach we investigated the effect of interstitial carbon and substitutional manganese on the structural and magnetic properties of bcc and fcc Fe. We concluded that neither manganese nor carbon at 3 at.% concentration changes the ground magnetic state of iron, which remains FM and AFMD (within the collinear spin configuration) for bcc and fcc Fe, respectively. Nonetheless, we find that the local magnetic interactions are strongly affected by carbon. Our calculations demonstrate that carbon frustrates the local magnetic order in fcc Fe by the spin reorientation of the nearest iron atoms and favors them to be ferromagnetically coupled. Carbon stabilizes the ferromagnetic Mn–Fe coupling in the Fe5MnC octahedron in bcc Fe, while in fcc Fe–Mn–C the orientation of manganese magnetic moment may have both antiferromagnetic and ferromagnetic coupling with the iron host.

Thus, our results demonstrate that antiferromagnetic fcc Fe–C and Fe–Mn–C alloys are intrinsically inhomogeneous magnetic systems due to the presence of carbon which favors the appearance of ferromagnetically ordered clusters and induces instability of the AFM state relative to the ferromagnetic one. These results may help explain the existence of ferromagnetic inhomogeneities and the increase in magnetic susceptibility with increasing carbon content in antiferromagnetic Fe–Mn–C alloys [41]. Furthermore, the competition of antiferromagnetic and ferromagnetic Fe–Fe and Fe–Mn interactions and the local magnetovolume instability near carbon lead to frustrated magnetic coupling which may be responsible for the spin-glass-like behavior observed in austenitic Fe–Mn–C alloys [41].

Acknowledgments

We thank Dr L Sandratskii for helpful discussion. The work is supported by the National Science Foundation (grant CMMI-0726888). NIM also acknowledges the support by the Russian Basic Research Foundation (grant no. 09-03-00070a).

References

[1] Scott C, Allain S, Faral M and Guelton N 2006 *Rev. Met. Paris* **103** 293
[2] Bhadeshia H K D H 2005 *Ironmak. Steelmak.* **32** 405
[3] Caballero F G, Bhadeshia H K D H, Mawella K J A, Jones D G and Brown P 2001 *Mater. Sci. Tech.* **17** 512–16
[4] Tsunoda Y 1989 *J. Phys.: Condens. Matter* **1** 10427
[5] Acet M, Zahres H, Wassermann E F and Pepperhoff W 1994 *Phys. Rev.* B **49** 6012
[6] Marcus P M, Moruzzi V L and Qiu S L 1999 *Phys. Rev.* B **60** 369
[7] Mryasov O N, Liechtenstein A I, Sandratskii L M and Gubanov V A 1991 *J. Phys.: Condens. Matter* **3** 7683
[8] Sandratskii L M and Kubler J 1992 *J. Phys.: Condens. Matter* **4** 6927
Uhl M, Sandratskii L M and Kubler J 1994 *Phys. Rev.* B **50** 291
[9] Antropov V P, Katsnelson M I, Harmon B N, van Schilfgaarde M and Kusnezov D 1996 *Phys. Rev.* B **54** 1019
[10] Kakehashi Y, Jepsen O and Kimura N 2002 *Phys. Rev.* B **65** 134418
[11] Knopfle K, Sandratskii L and Kubler J 2000 *Phys. Rev.* B **62** 5564
[12] Sjostedt E and Nordstrom L 2002 *Phys. Rev.* B **66** 014447
[13] Wang C S, Klein B M and Krakauer H 1985 *Phys. Rev. Lett.* **54** 1852
[14] Moruzzi V L, Marcus P M and Kubler J 1989 *Phys. Rev.* B **39** 6957
[15] Singh D J, Pickett W E and Krakauer H 1991 *Phys. Rev.* B **43** 11628
[16] Amador C, Lambrecht W R L and Segall B 1992 *Phys. Rev.* B **46** 1870
[17] Herper H C, Hoffmann E and Entel P 1999 *Phys. Rev.* B **60** 3839
[18] Garcia-Suarez V M, Newman C M, Lambert C J, Pruneda J M and Ferrer J 2004 *Eur. Phys. J.* B **40** 371
[19] Abrikosov I A, Kissavos A E, Liot F, Alling B, Simak S I, Peil O and Ruban A V 2007 *Phys. Rev.* B **76** 014434
[20] Acet M, Shneider Th, Gehrmann B and Wassermann E F 1995 *J. Physique IV Colloq.* **C8** 379
[21] Radhakrishna P and Livet F 1978 *Solid State Commun.* **25** 597
[22] Child H R and Cable J W 1976 *Phys. Rev.* B **13** 227
[23] Kajzar F and Parette G 1980 *Phys. Rev.* B **22** 5471
[24] Drittler B, Stefanou N, Blugel S, Zeller R and Dederichs P H 1989 *Phys. Rev.* B **40** 8203
[25] Anisimov V I, Antropov V P, Liechtenstein A I, Gubanov V A and Postnikov A V 1988 *Phys. Rev.* B **37** 5598
[26] Kulikov N I and Demangeat C 1997 *Phys. Rev.* B **55** 3533

[27] Mirzoev A A, Yalalov M M and Mirzaev D A 2006 *Phys. Met. Metallogr.* **101** 341
[28] Ishikawa Y 1968 *J. Appl. Phys.* **39** 1318
Endoh Y and Ishikawa Y 1971 *J. Phys. Soc. Japan* **30** 1614
[29] Podgorny M 1992 *Phys. Rev.* B **45** 797
[30] Kubler J, Hock K H, Sticht J and Williams A R 1988 *J. Phys. F: Met. Phys.* **18** 469
[31] Spisa'k D and Hafner J 2000 *Phys. Rev.* B **61** 11569
[32] Akbar S and Kimura N 1998 *J. Phys.: Condens. Matter* **10** 2081
[33] Pepperhoff W and Acet M 2001 *Constitution and Magnetism of Iron and Its Alloys* (Berlin: Springer)
[34] Timoshevskii A N, Timoshevskii V A and Yanchitsky B Z 2001 *J. Phys.: Condens. Matter* **13** 1051
[35] Elzain M E, Yousif A A and Pollak H 1996 *J. Phys. Chem. Sol.* **57** 297
[36] Oda K, Fujimura H and Ino H 1994 *J. Phys.: Condens. Matter* **6** 679
[37] Shanina B D, Gavriljuk V G, Konchitz A A and Kolesnik S P 2000 *Physica* B **284** 1313
[38] Gavriljuk V G, Kucherenko Yu N, Moravetsky V I, Nadutov V M and Sheludchenko L M 1994 *J. Phys. Chem. Solids* **55** 1181
[39] Jiang D E and Carter E A 2003 *Phys. Rev.* B **67** 214103
[40] Boukhvalov D W, Gornostyrev Yu N, Katsnelson M I and Lichtenstein A I 2007 *Phys. Rev. Lett.* **99** 247205
[41] Stamm W, Zähres H, Acet M, Schletz K and Wassermann E F 1988 *J. Physique Colloq.* C8 **49** 315
[42] Drittler B, Stefanou N, Blugel S, Zeller R and Dederichs P H 1989 *Phys. Rev.* B **40** 8203
[43] Kresse G and Hafner J 1993 *Phys. Rev.* B **48** 13115
[44] Kresse G and Furthmuller J 1996 *Phys. Rev.* B **54** 11169
[45] Perdew J P, Burke K and Ernzerhof M 1996 *Phys. Rev. Lett.* **77** 3865
[46] Acet M, Gehrmann B, Wassermann E F, Bach H and Pepperhoff W 2001 *J. Magn. Magn. Mater.* **232** 221
[47] Acet M, Wassermann E F and Pepperhoff W 2000 *Phil. Mag.* B **80** 127
[48] van Schilfgaarde M, Abrikosov I A and Johansson B 1999 *Nature* **400** 46
[49] Hadfield R and Burnham T H 1933 *Special Steels* 2nd edn (New York: The Pitman Press) p 100
[50] Hasegawa H and Pettifor D G 1983 *Phys. Rev. Lett.* **50** 130
[51] Andersen O K, Jepsen O and Sob M 1986 *Electronic Band Structure and its Applications* ed M Yussouff (Berlin: Springer)
[52] Lichtenstein A I, Zaanen J and Anisimov V I 1995 *Phys. Rev.* B **52** R5467